

# The $\gamma$ - $\alpha$ iso-structural Transition in Cerium, a Critical Element

Nicola Lanatà,<sup>1,\*</sup> Yong-Xin Yao,<sup>2,\*</sup> Cai-Zhuang Wang,<sup>2</sup>  
Kai-Ming Ho,<sup>2</sup> Jörg Schmalian,<sup>3</sup> Kristjan Haule,<sup>1</sup> and Gabriel Kotliar<sup>1</sup>

<sup>1</sup>*Department of Physics and Astronomy, Rutgers University, Piscataway, New Jersey 08856-8019, USA*

<sup>2</sup>*Ames Laboratory-U.S. DOE and Department of Physics and Astronomy,  
Iowa State University, Ames, Iowa IA 50011, USA*

<sup>3</sup>*Karlsruhe Institute of Technology, Institute for Theory of Condensed Matter, D-76131 Karlsruhe, Germany*

(Dated: August 28, 2018)

**Below the critical temperature  $T_c \simeq 600K$ , an iso-structural transition, named  $\gamma$ - $\alpha$  transition, can be induced in Cerium by applying pressure. This transition is first-order, and is accompanied by a sizable volume collapse. A conclusive theoretical explanation of this intriguing phenomenon has still not been achieved, and the physical pictures proposed so far are still under debate. In this work, we illustrate zero-temperature first-principle calculations which clearly demonstrate that the  $\gamma$ - $\alpha$  transition is induced by the interplay between the electron-electron Coulomb interaction and the spin-orbit coupling. We address the still unresolved problem on the existence of a second low- $T$  critical point, i.e., whether the energetic effects alone are sufficient or not to induce the  $\gamma$ - $\alpha$  transition at zero temperature.**

The  $\gamma$ - $\alpha$  iso-structural transition in Cerium [1] was discovered in 1949 [2]. Since then, a lot of theoretical and experimental work has been devoted to its understanding. The great interest in this phenomenon arises from the fact that the transition is isostructural, i.e., the lattice structure of the system is equal in the two phases. Furthermore, the possibility that the underlying mechanism lies in the electronic structure only — i.e., without it being necessary to involve other effects — makes Cerium a potential theoretical testing ground for basic concepts of correlated electron systems. Two main theoretical pictures are still under debate to explain the volume collapse: the Kondo volume collapse (KVC) [3, 4] and the orbital-selective Mott transition within the Hubbard model (HM) [5]. According to the KVC the transition is induced by the rapid change of the coherence temperature across the transition boundaries, which affect dramatically the structure of the conduction *spd* electrons through Kondo effect. According to the HM, instead, it is the hopping between *f* orbitals that changes drastically across the transition between the  $\alpha$  phase (with delocalized *f* electrons) and the  $\gamma$  phase (with localized *f* electrons), as for the Mott transition in the Hubbard model.

Consistently with both the HM and the KVC pictures, the *f*-electrons are strongly correlated both in the  $\alpha$  and in the  $\gamma$  phase. This fact is clearly indicated, e.g., by the photoemission spectra, which is known experimentally [6–8] and theoretically [9–11]. Despite this similarity, there is a key difference between these two models: while the KVC attributes a very important role to the interplay between the localized *4f* orbitals and the itinerant *spd* conduction bands, the itinerant electrons are “spectators” in the HM picture.

The development of LDA+DMFT (Local Density Approximation plus Dynamical Mean Field Theory) [12] re-

sults [13–15] has successfully reproduced many aspects of this transition, and different aspects of these studies can be understood in both physical pictures. There are still fundamental questions which have not been answered. (1) What is the role of the spin-orbit interaction (SOC) for the volume-collapse? (2) What is the fate of the pressure-temperature transition-line at very low temperatures [16–18]? (3) Can a first-principle based theory be made computationally efficient so as to access both the  $\gamma$  and the  $\alpha$  Cerium at zero temperature?

Due to the complexity of the problem, it is clear that, in order to be conclusive, a theoretical explanation of the  $\gamma$ - $\alpha$  transition needs to be supported by first-principles calculations which, not only are able to take into account both the details of the band-structure and the strong-correlation effects, but are also able to evaluate precisely the pressure-volume phase diagram. For this purpose, it is crucial that the computation of the total energy is essentially free of numerical error. Another key requirement is that the two phases are treated within the same theoretical framework. In this work, we use a combination of Density Functional Theory and the Gutzwiller Approximation (LDA+GA) [19–23], which satisfies all of these requirements. Recently, we have established formally [L.N. et al.] that this method can be viewed as an instance of LDA+DMFT, using Slave Bosons (or the Gutzwiller method) as the DMFT impurity solver [14]. This insight enabled a new efficient charge self-consistent implementation of the LDA+GA method on top [Y.Y.X. et al.] of the LAPW DFT code Wien2k [24], which removes many of the approximations inherent in previous studies. As a benchmark, in the supplementary material we present also LDA+DMFT calculations for Cerium. The very good agreement between the two methods gives us further confirmation that the results presented in this work are indeed reliable.

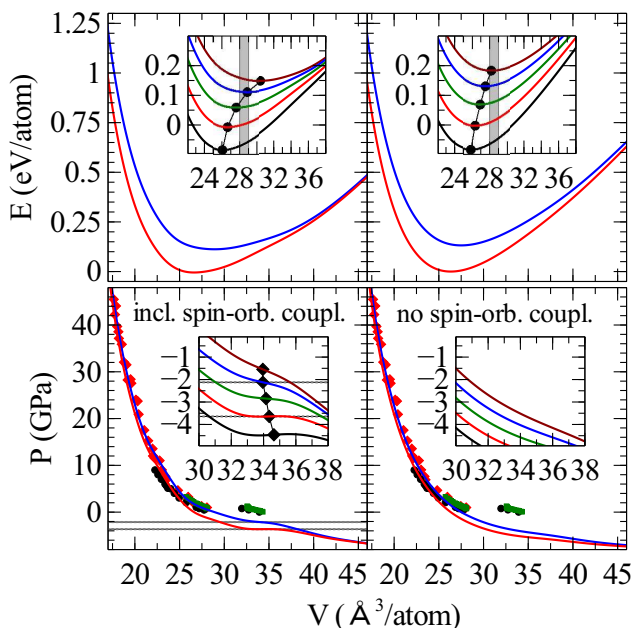


FIG. 1: Total energy as a function of the volume (upper panels) and corresponding theoretical pressure-volume curves for  $U = 5, 6 \text{ eV}$ ,  $J = 0.7 \text{ eV}$ , in comparison with the experimental data (lower panels). The experimental data relate to measurements at room temperature (black circles from Ref. [27], red diamonds from Ref. [28] and green squares from Ref. [29]), while our theoretical calculations are all obtained at zero temperature. The curves in the insets are obtained for all  $U$ 's from  $4.5 \text{ eV}$  to  $6.5 \text{ eV}$  (from lower to higher total energies) with step of  $0.5 \text{ eV}$ . Our results are shown both with (left panels) and without (right panels) taking into account the spin-orbit coupling. The vertical shaded line in the upper insets indicate the experimental volume at ambient pressure. The horizontal dotted lines in the lower-left panel and the black diamonds in its inset indicate the pressures where the bulk-modulus  $\mathcal{K} = -VdP/dV$  is minimum.

We employ the general Slater-Condon parametrization of the on-site interaction, assuming a Hund's coupling constant  $J = 0.7 \text{ eV}$  [25]. Since the value  $U$  of the interaction strength is generally difficult to establish accurately (due to its strong sensitivity to the screening effect), in this work we perform calculations scanning different values of  $U$ . Our calculations are all performed at zero temperature.

In the upper panels of Fig. 1 we illustrate our theoretical energy-volume diagrams for different values of  $U$ . The results are shown both by taking into account the SOC (left panels) and by neglecting it in the calculation (right panels). The corresponding pressure-volume curves, obtained from  $P = -dE/dV$ , are shown in the lower panels, in comparison with the experimental data at room temperature of Refs. [27, 28]. The agreement with the experiment is good, especially for  $U = 6 \text{ eV}$ , which is the value that reproduces the experimental equilibrium-

volume  $V_{\text{eq}} \simeq 28.5 \text{ Å}^3/\text{atom}$  [26–28] (see the inset of the higher-left panel). The small discrepancies at larger  $V$  are likely, at least in part, due to the entropy, as our calculations were performed at zero temperature. Note that  $U = 6 \text{ eV}$  was also previously computed within the constrained LDA method [9, 30], which gives us further confidence that this is the optimal value of the correlation strength for Cerium.

Remarkably, we observe a change of sign in the bulk-modulus  $\mathcal{K} = -VdP/dV < 0$  — which is the signal of a first-order iso-structural transition — for any  $U \leq U_c \simeq 5.5 \text{ eV}$  (see the pressure-volume curves in the lower-panels insets of Fig. 1); while at  $U = U_c$  the transition becomes second-order, with  $\mathcal{K} = 0$  minimum bulk-modulus. A signature of the transition, i.e., a local minimum of the bulk-modulus, is still present for any interaction strength, see the black diamonds in the inset of the lower-left panel of Fig. 1. We point out that this feature of the pressure-volume curve is observed *only* if the SOC is taken into account — which is a clear indication of its key role in the physics underlying the  $\gamma$ - $\alpha$  transition. Note also that, for  $U = 6 \text{ eV}$ , the crossover point occurs at  $P \simeq -2 \text{ Gp}$ , which is close to the expected zero-temperature value  $P_{\text{exp}} \simeq -1 \text{ Gp}$  extrapolated from the experimental data of Ref. [1].

In order to better understand the role of the SOC, we consider the local  $f$  entanglement entropy,

$$S_f[\rho_f] = -\text{Tr}[\rho_f \ln \rho_f] , \quad (1)$$

where  $\rho_f$  is the reduced density matrix of the system in the  $f$  local subspace. The value of  $S_f$  is a measure of how much the  $f$  electrons are entangled with the rest of the environment. In Fig. 2 the behaviour of  $S_f$  is shown as a function of the volume for two values of  $U$ . Remarkably, if (and only if) the SOC is taken into account, a clear crossover is visible in correspondence of the signature of the volume collapse, i.e., in correspondence of the minimum of the bulk-modulus  $\mathcal{K}$ , which is indicated by black diamonds in the inset of the lower-left panel of Fig. 1.

In the  $\alpha$  phase, as expected,  $S_f$  is not sensitive to the spin-orbit splitting, indicating that the local fluctuations induced in the  $f$  local space by the coupling with its environment are very large. By increasing the volume, the fluctuations between the  $J = 5/2 \ f^1$  subspace and the other local configurations are increasingly suppressed. The crossover point identifies the situation in which the above-mentioned fluctuations are sufficiently small to be hampered by the spin-orbit splitting. This is clearly demonstrated by the fact that in the  $\gamma$  phase, when the SOC is taken into account,  $S_f \gtrsim \ln 6$  — where  $6 = 2 \times 5/2 + 1$  is the degeneracy of the  $5/2$  eigenspace at  $n_f = 1$ . We point out that the above-mentioned local fluctuations are generated only by the entanglement, and so are present even if the actual temperature of the system is zero — as in our calculations. As we are going to

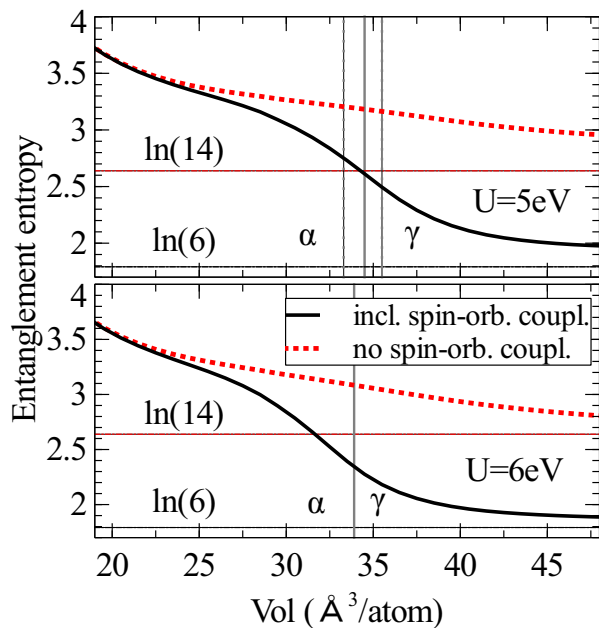


FIG. 2: Local entanglement entropy of the  $f$ -electrons as a function of the volume per atom of the system for  $U = 5 \text{ eV}$  (upper panel) and  $U = 6 \text{ eV}$  (lower panel) at fixed  $J = 0.7 \text{ eV}$ . The entanglement entropy is reported both for the case with (lines) and without (dots) the SOC. The horizontal lines correspond to 14, which is the dimension of the single-particle local space of the  $f$ -electrons, and to  $6 = 2 \times 5/2 + 1$ , which is the degeneracy of the  $5/2$   $f$ -electrons within the single-particle local space. The vertical continue lines indicate the signature of the transition in the pressure-volume diagram, and the dotted vertical lines indicate the boundary of the  $\gamma$ - $\alpha$  transition (which occurs only for  $U \leq U_c \simeq 5.5 \text{ eV}$ ) according to the equal-area construction [31].

show, the main source of entanglement is the hybridization between the  $f$  and the  $spd$  electrons.

A further insight of the problem can be achieved by inspecting the ground-state expectation values of the non-local energy components of the effective Hamiltonian  $\hat{\mathcal{H}}$  whose ground-state provides our theoretical solution [12, 21]. The non-local part  $\hat{T}$  of  $\hat{\mathcal{H}}$  can be concisely represented as

$$\hat{T} = \hat{T}_{ff} + \hat{T}_{fc} + \hat{T}_{cc}, \quad (2)$$

where the symbol  $c$  represents all of the  $spd$  conduction electrons, and  $\hat{T}_{ff}$ ,  $\hat{T}_{fc}$  and  $\hat{T}_{cc}$  represent the non-local “hopping” terms between  $f$ - $f$ ,  $f$ - $c$  and  $c$ - $c$  electrons, respectively. In Fig. 3 the ground-state expectation values of the  $f$ - $c$  and the  $f$ - $f$  components of  $\hat{T}$  are shown for two values of  $U$ . These energies represent the Kondo and the Hubbard energy scales of the problem, respectively. In agreement with the KVC model of the transition, we observe that the Kondo energy scale is about one order of magnitude bigger than the Hubbard energy scale, which is already very small before the crossover point, as ex-

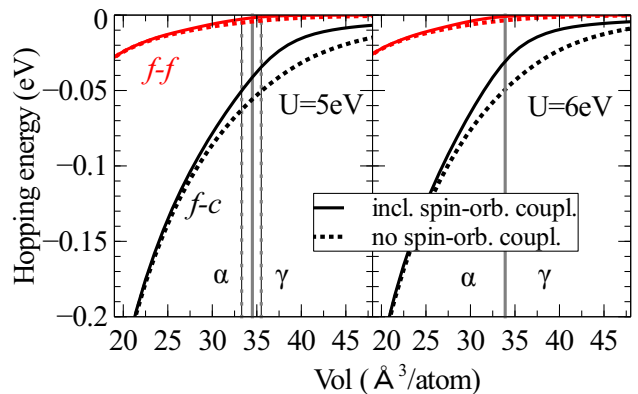


FIG. 3: Ground-state expectation values of the  $f$ - $c$  and the  $f$ - $f$  effective hopping energies as a function of the volume per atom of the system. The energies are reported for  $U = 5 \text{ eV}$  (left panel) and  $U = 6 \text{ eV}$  (right panel) at fixed  $J = 0.7 \text{ eV}$ , both for the case with (lines) and without (dots) the spin-orbit coupling. The vertical continue lines indicate the signature of the transition in the pressure-volume diagram, and the dotted vertical lines indicate the boundary of the  $\gamma$ - $\alpha$  transition (which occurs only for  $U \leq U_c \simeq 5.5 \text{ eV}$ ) according to the equal-area construction [31].

pected [32]. This confirms that the main source of entanglement between the  $f$  local space and its environment is the hybridization between the  $f$  and the  $spd$  electrons. Note that, when the SOC is taken into account, a more rapid suppression of the Kondo energy scale is observed concomitantly with the crossover region.

We have already observed that, even though the behaviour of the entanglement entropy (and of the Kondo energy scale) are qualitatively the same for all  $U$ 's, no transition can be found for  $U \geq U_c \simeq 5.5 \text{ eV}$  at zero temperature, see Figs. 1 and 2. The reason is the following. The local crossover, which induces a reduction of the bulk-modulus of the system, occurs at lower volumes for larger  $U$ , see the black diamonds in the inset of the lower-left panel of Fig. 1. On the other hand, the bulk-modulus becomes larger at smaller volumes (even when the SOC is not taken into account), see the pressure-volume curves in the lower panels of Fig. 1. For this reason, if  $U$  is large enough, it becomes impossible for the SOC to make the bulk-modulus negative, i.e., to induce the volume collapse. It follows that, in principle, there are two possible scenarios: (i) the  $\gamma$ - $\alpha$  transition exists also at zero temperature, or (ii) the transition line ends at a certain finite critical temperature (at negative pressures). As we mentioned before,  $U \simeq 6 \text{ eV}$  — which is indeed very close to  $U_c$  — is a physically reasonable value for Cerium. This suggests that Cerium is placed essentially in the middle between the two above-mentioned scenarios, i.e., that the  $\gamma$ - $\alpha$  transition line ends very close to zero temperature. Note that this finding is in qualitative agreement with the experimental results of Ref. [33].

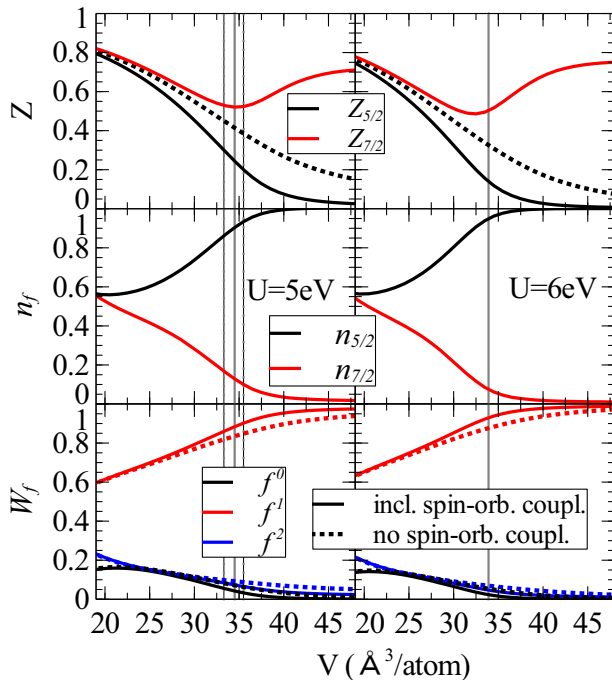


FIG. 4: Quasi-particle renormalization weights of the 7/2 and 5/2  $f$ -electrons (upper panels), 7/2 and 5/2  $f$  orbital populations (central panels), and  $f$  configuration probabilities (lower panels), as a function of the volume of the system. The renormalization weights and the configuration probabilities are reported both for the case with and without the spin-orbit coupling, for  $U = 5 \text{ eV}$  (left panels) and  $U = 6 \text{ eV}$  (right panels) at fixed  $J = 0.7 \text{ eV}$ . The vertical continue lines indicate the signature of the transition in the pressure-volume diagram, and the dotted vertical lines indicate the boundary of the  $\gamma$ - $\alpha$  transition (which occurs only for  $U \leq U_c \simeq 5.5 \text{ eV}$ ) according to the equal-area construction [31].

It is useful to examine how the local crossover induced by the SOC reflects on the quasi-particle renormalization weights and the on-site configuration probabilities. In the first panel of Fig. 4 are illustrated the averaged quasi-particle renormalization weights  $Z$  of the 7/2 and 5/2  $f$ -electrons — which are significantly different because of the spin-orbit effect. As expected [32], the  $f$ -electrons are correlated ( $Z$  is significantly smaller than 1) even in the  $\alpha$  phase, and the two  $Z$ 's monotonically decrease by increasing the volume at higher pressures. Nevertheless, they develop a qualitatively different behaviour at the crossover point. While the 5/2 electrons undergo a clear crossover toward a localized phase “disentangled” by the conduction electrons, the 7/2 electrons remain screened, but they rapidly disappear afterwards, so that they are essentially absent in the  $\gamma$  phase, see the second panel of Fig. 4. As shown by the  $f$  configuration probabilities in the third panel of Fig. 4, the SOC speeds up the formation of the  $4f^1$  local moment. In other words, the SOC acts as a “catalyst”, which favors the disentanglement

between the  $4f$  electrons and the conduction electrons.

In conclusion, we have performed first principle calculations on Cerium using a new efficient implementation of the LDA+GA method. For the physical value of  $U$  in Cerium,  $U \simeq 6 \text{ eV}$  [9, 30], a sharp crossover is observed in many physical quantities around the volume where the bulk-modulus is minimum. This finding is robust against changes in  $U$ , but the details are different. For  $U < U_c$ , at  $T = 0$ , there is a first-order transition at a given negative value of the pressure, while for  $U > U_c$  this transition becomes a sharp crossover. At  $U_c$  there is a second-order quantum critical point in the phase diagram. Our estimate for the critical interaction strength,  $U_c \simeq 5.5 \text{ eV}$ , is very close to the physical value of the interaction strength in Cerium. This finding suggests that elemental Cerium is a critical element, consistently with the experiments [33]. Our results demonstrate the importance of the SOC for the volume collapse in Cerium, which is neatly captured by the rapid variation of the entanglement entropy of the  $f$ -electrons in the region around the minimum of the bulk-modulus. In the  $\alpha$  phase, at small  $V$ , the  $f$ -levels are strongly hybridized with the conduction electrons, and the quasiparticle weights and the pressure are only weakly-dependent on the spin-orbit interaction. In this regime the system effectively behaves as if the  $f$ -level degeneracy was of the order of magnitude of 14. In the  $\gamma$  phase, at large  $V$ , the spin-orbit splitting becomes more important, and substantially reduces the effective  $f$ -level degeneracy. The fact that the quasi-particle weight in the  $\gamma$  phase is much smaller when the SOC is taken into account, see Fig. 4, can be interpreted as a consequence of the above-mentioned reduction of effective  $f$ -level degeneracy — a well known effect in the theory of the single-ion Kondo impurity. As in the early Kondo volume collapse theory [3],  $\partial Z / \partial V$  contributes to the pressure. However, some qualitative features of our solution, such as the form of the pressure-volume phase diagram, show that other physical elements, such as the changes in the charge density induced by the correlations, have to also be included in realistic theories of this material.

## CONTRIBUTIONS

N.L. and Y.X.Y. co-developed the GA code and analyzed the data. N.L. developed the theoretical explanation of the iso-structural transition, wrote the manuscript and carried out the LDA+DMFT benchmark calculations. Y.X.Y., C.Z.W. and K.M.H. initiated the project and carried out the LDA+GA calculations. Y.X.Y. edited the figures, and coded the interface between Wien2k and the GA solver, which was constructed on the basis of the LDA+DMFT interface developed by K.H.. K.H. developed the DMFT code. G.K. and J.S. proposed the project and supervised the



research. All the authors provided fundamental insights, and contributed to improve the manuscript.

**Corresponding author:** Y.X.Yao; ykent@iastate.edu

## ACKNOWLEDGMENTS

N.L. and Y.X.Y. thank XiaoYu Deng and Robert McQueeney for useful discussion. The collaboration was supported by the U.S. Department of Energy through the Computational Materials and Chemical Sciences Network CMSCN. Research at Ames Laboratory supported by the U.S. Department of Energy, Office of Basic Energy Sciences, Division of Materials Sciences and Engineering. Ames Laboratory is operated for the U.S. Department of Energy by Iowa State University under Contract No. DE-AC02-07CH11358.

---

\* Equally contributed to this work

- [1] Koskenmaki, D. C. & Jr., K. A. G. Chapter 4 cerium. In Karl A. Gschneidner, J. & Eyring, L. (eds.) *Metals*, vol. 1 of *Handbook on the Physics and Chemistry of Rare Earths*, 337 – 377 (Elsevier, 1978).
- [2] Lawson, A. W. & Tang, T.-Y. Concerning the high pressure allotropic modification of cerium. *Phys. Rev.* **76**, 301–302 (1949).
- [3] Allen, J. W. & Martin, R. M. Kondo volume collapse and the  $\gamma \rightarrow \alpha$  transition in cerium. *Phys. Rev. Lett.* **49**, 1106–1110 (1982).
- [4] Lavagna, M., Lacroix, C. & Cyrot, M. Volume collapse in the kondo lattice. *Phys. Lett. A* **90**, 210 – 212 (1982).
- [5] Johansson, B. The  $\alpha$ - $\gamma$  transition in cerium is a mott transition. *Philos. Mag.* **30**, 469 (1974).
- [6] Wieliczka, D. M., Olson, C. G. & Lynch, D. W. Valence-band photoemission in la and pr: Connections with the Ce problem. *Phys. Rev. Lett.* **52**, 2180–2182 (1984).
- [7] Weschke, E. *et al.* Surface and bulk electronic structure of Ce metal studied by high-resolution resonant photoemission. *Phys. Rev. B* **44**, 8304–8307 (1991).
- [8] Patthey, F., Delley, B., Schneider, W. D. & Baer, Y. Low-energy excitations in  $\alpha$ - and  $\gamma$ -ce observed by photoemission. *Phys. Rev. Lett.* **55**, 1518–1521 (1985).
- [9] Zöfl, M. B., Nekrasov, I. A., Pruschke, T., Anisimov, V. I. & Keller, J. Spectral and magnetic properties of  $\alpha$ - and  $\gamma$ -Ce from dynamical mean-field theory and local density approximation. *Phys. Rev. Lett.* **87**, 276403 (2001).
- [10] Held, K., McMahan, A. K. & Scalettar, R. T. Cerium volume collapse: Results from the merger of dynamical mean-field theory and local density approximation. *Phys. Rev. Lett.* **87**, 276404 (2001).
- [11] McMahan, A. K., Held, K. & Scalettar, R. T. Thermodynamic and spectral properties of compressed Ce calculated using a combined local-density approximation and dynamical mean-field theory. *Phys. Rev. B* **67**, 075108 (2003).
- [12] Kotliar, G. *et al.* Electronic structure calculations with dynamical mean-field theory. *Rev. Mod. Phys.* **78**, 865 (2006).
- [13] Haule, K., Oudovenko, V., Savrasov, S. Y. & Kotliar, G. The  $\alpha \rightarrow \gamma$  transition in ce: A theoretical view from optical spectroscopy. *Phys. Rev. Lett.* **94**, 036401 (2005).
- [14] Kotliar, G. *et al.* Electronic structure calculations with dynamical mean-field theory. *Rev. Mod. Phys.* **78**, 865–951 (2006).
- [15] Moore, K. T. & van der Laan, G. Nature of the 5f states in actinide metals. *Rev. Mod. Phys.* **81**, 235–298 (2009).
- [16] de’ Medici, L., Georges, A., Kotliar, G. & Biermann, S. Mott transition and kondo screening in f-electron metals. *Phys. Rev. Lett.* **95**, 066402 (2005).
- [17] Amadon, B., Biermann, S., Georges, A. & Aryasetiawan, F. The  $\alpha$ - $\gamma$  transition of cerium is entropy driven. *Phys. Rev. Lett.* **96**, 066402 (2006).
- [18] Casadei, M., Ren, X., Rinke, P., Rubio, A. & Scheffler, M. Density-functional theory for f-electron systems: The  $\alpha$ - $\gamma$  phase transition in cerium. *Phys. Rev. Lett.* **109**, 146402 (2012).
- [19] Gutzwiller, M. C. Correlation of electrons in a narrow s band. *Phys. Rev.* **137**, A1726–A1735 (1965).
- [20] Zein, N. E. Correlation energy functionals for *ab initio* calculations: Application to transition metals. *Phys. Rev. B* **52**, 11813–11824 (1995).
- [21] Deng, X., Wang, L., Dai, X. & Fang, Z. Local density approximation combined with gutzwiller method for correlated electron systems: Formalism and applications. *Phys. Rev. B* **79**, 075114 (2009).
- [22] Ho, K. M., Schmalian, J. & Wang, C. Z. Gutzwiller density functional theory for correlated electron systems. *Phys. Rev. B* **77**, 073101 (2008).
- [23] Lanatà, N., Strand, H. U. R., Dai, X. & Hellsing, B. Efficient implementation of the gutzwiller variational method. *Phys. Rev. B* **85**, 035133 (2012).
- [24] Blaha, P., Schwarz, K., Madsen, G., Kvasnicka, D. & Luitz, J. *An augmented plane wave plus local orbitals program for calculating crystal properties*. University of Technology, Vienna (2001).
- [25] Cowan, R. D. *The Theory of Atomic Structure and Spectra* (University of California Press, Berkeley, 1981).
- [26] Ellinger, F. H. & Zachariasen, W. H. Structure of cerium metal at high pressure. *Phys. Rev. Lett.* **32**, 773–774 (1974).
- [27] Zachariasen, W. H. & Ellinger, F. H. The crystal structures of cerium metal at high pressure. *Acta Crystallogr. Sec. A* **33**, 155–160 (1977).
- [28] Olsen, J., Gerward, L., Benedict, U. & Itié, J.-P. The crystal structure and the equation of state of cerium metal in the pressure range 0-46 GPa. *Physica B+C* **133**, 129–137 (1985).
- [29] Lipp, M. J. *et al.* X-ray emission spectroscopy of cerium across the  $\gamma$ - $\alpha$  volume collapse transition. *Phys. Rev. Lett.* **109**, 195705 (2012).
- [30] McMahan, A., Huscroft, C., Scalettar, R. & Pollock, E. Volume-collapse transitions in the rare earth metals. *Journal of Computer-Aided Materials Design* **5**, 131–162 (1998).
- [31] Landau, L. D. & Lifshitz, E. M. *Statistical Physics* (Peramon, London, 1958).
- [32] Murani, A. P., Levett, S. J. & Taylor, J. W. Magnetic form factor of  $\alpha$ -ce: Towards understanding the magnetism of cerium. *Phys. Rev. Lett.* **95**, 256403 (2005).

- [33] Lashley, J. C. *et al.* Tricritical phenomena at the  $\gamma \rightarrow \alpha$  transition in  $\text{Ce}_{0.9-x}\text{La}_x\text{Th}_{0.1}$  alloys. *Phys. Rev. Lett.* **97**, 235701 (2006).

## SUPPLEMENTARY MATERIAL

### METHODS

In our LDA+GA code the LDA calculations are performed by Wien2k [1], which is an all-electron DFT package based on the full-potential (linearized) augmented plane-wave ((L)APW)+local orbitals (lo) method. A key advantage of this package is that it is one among the most accurate schemes for band-structure calculations, and it is free of any numerical error due to the frozen-core pseudopotentials or from the downfolding, which have been used in previous implementations of the LDA+GA method.

Our new LDA+GA implementation, to be described in a longer publication [Y.Y.X. et al.], is patterned after the LDA+DMFT work of Ref. [2]. Using the same interface, basis set, projectors onto the correlated orbitals, enables a meaningful comparison between the two methods. We have employed a new numerical implementation of the GA solver [L.N. et. al, Strand Hugo U.R. et. al], which further improves the method previously proposed in Ref. [3], and is a generalization of earlier formulations of the GA [4–8].

### LDA+DMFT BENCHMARK CALCULATIONS

The purpose of this section is to benchmark our LDA+GA calculations within the LDA+DMFT method, using the Continuous Time Quantum Monte Carlo method (CTQMC) [9] — which is numerically-exact — as the impurity solver. We use the implementation of Ref [10].

Our DMFT calculations are all performed at  $T = 58 K$ , while the GA calculations are done at zero temperature.

In Fig. 5 are shown the local configuration probabilities (upper panels) and the  $f$  entanglement entropy (lower panels) as a function of the volume, for two different values of  $U$ . The agreement between the two methods is indeed very good. In particular, we point out that the  $f$  local crossover, which is indicated by the rapid change of the corresponding entanglement entropy, is clearly visible also within the LDA+DMFT method.

In Fig. 6 it is shown the evolution of the quasi-particle renormalization weights as a function of the volume (upper panels) and the imaginary part of the self-energy at the Fermi level (lower panels). Note that in the  $\gamma$  phase, i.e., after the local crossover, the 5/2 electrons are no longer coherent. For this reason, at the temperature at which our DMFT calculations have been carried out,  $Z_{5/2}$  is not well defined at large volumes.

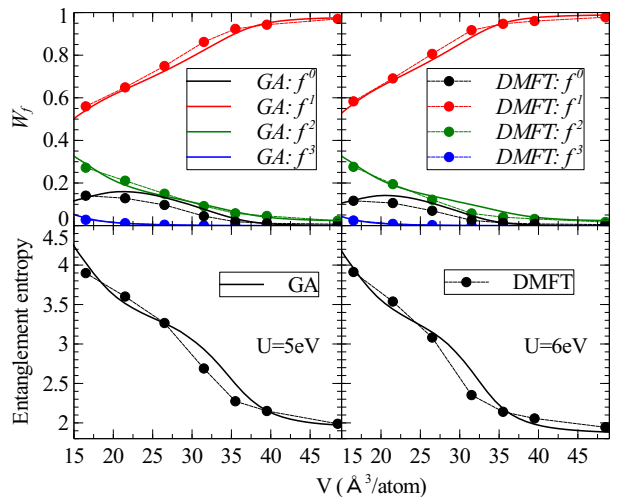


FIG. 5: Local configuration weights (upper panels) and  $f$  entanglement entropy (lower panels). Comparison between LDA+GA (lines) and LDA+DMFT (dots) results for  $U = 5 eV$  (left panels) and  $U = 6 eV$  (right panels) at fixed  $J = 0.7 eV$ .

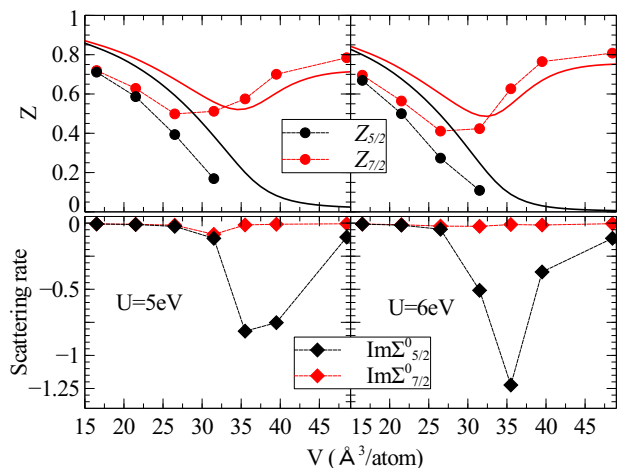


FIG. 6: Quasi-particle renormalization weights of the 7/2 and 5/2  $f$ -electrons (upper panels), and imaginary part of the self-energy at the Fermi level (lower panels). Comparison between LDA+GA (lines) and LDA+DMFT results (dots) for  $U = 5 eV$  (left panels) and  $U = 6 eV$  (right panels) at fixed  $J = 0.7 eV$ .

\* Equally contributed to this work

- [1] Blaha, P., Schwarz, K., Madsen, G., Kvasnicka, D. & Luitz, J. *An augmented plane wave plus local orbitals program for calculating crystal properties*. University of Technology, Vienna (2001).
- [2] Haule, K., Yee, C.-H. & Kim, K. Dynamical mean-field theory within the full-potential methods: Electronic structure of CeIrIn<sub>5</sub>, CeCoIn<sub>5</sub>, and CeRhIn<sub>5</sub>. *Phys. Rev. B* **81**, 195107 (2010).

- [3] Lanatà, N., Strand, H. U. R., Dai, X. & Hellsing, B. Efficient implementation of the gutzwiller variational method. *Phys. Rev. B* **85**, 035133 (2012).
- [4] Fabrizio, M. Gutzwiller description of non-magnetic Mott insulators: Dimer lattice model. *Phys. Rev. B* **76**, 165110 (2007).
- [5] Lanatà, N., Barone, P. & Fabrizio, M. Fermi-surface evolution across the magnetic phase transition in the Kondo lattice model. *Phys. Rev. B* **78**, 155127 (2008).
- [6] Lanatà, N., Barone, P. & Fabrizio, M. Superconductivity in the doped bilayer hubbard model. *Phys. Rev. B* **80**, 224524 (2009).
- [7] Deng, X., Wang, L., Dai, X. & Fang, Z. Local density approximation combined with gutzwiller method for correlated electron systems: Formalism and applications. *Phys. Rev. B* **79**, 075114 (2009).
- [8] Büinemann, J., Weber, W. & Gebhard, F. Multiband gutzwiller wave functions for general on-site interactions. *Phys. Rev. B* **57**, 6896–6916 (1998).
- [9] Werner, P., Comanac, A., de’ Medici, L., Troyer, M. & Millis, A. J. Continuous-time solver for quantum impurity models. *Phys. Rev. Lett.* **97**, 076405 (2006).
- [10] Haule, K. Quantum monte carlo impurity solver for cluster dynamical mean-field theory and electronic structure calculations with adjustable cluster base. *Phys. Rev. B* **75**, 155113 (2007).